Journal Pre-proof

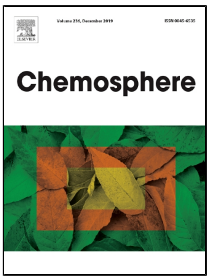

Tracing geochemical pollutants in stream water and soil from mining activity in an alpine catchment

Jianguo Li, Zongxing Li, Kate J. Brandis, Jianwei Bu, Ziyong Sun, Qiang Yu, Daniel Ramp

PII:	S0045-6535(19)32406-3
DOI:	https://doi.org/10.1016/j.chemosphere.2019.125167
Reference:	CHEM 125167
To appear in:	*Chemosphere*
Received Date:	11 March 2019
Accepted Date:	20 October 2019

Please cite this article as: Jianguo Li, Zongxing Li, Kate J. Brandis, Jianwei Bu, Ziyong Sun, Qiang Yu, Daniel Ramp, Tracing geochemical pollutants in stream water and soil from mining activity in an alpine catchment, *Chemosphere* (2019), https://doi.org/10.1016/j.chemosphere.2019.125167

Tracing geochemical pollutants in stream water and soil from mining activity in an alpine catchment

Jianguo Li [a], Zongxing Li [b, *], Kate J. Brandis [c], Jianwei Bu [d], Ziyong Sun [d], Qiang Yu [e], Daniel Ramp [a,*]

[a] Centre for Compassionate Conservation, Faculty of Science, University of Technology Sydney, Ultimo 2007 NSW, Australia

[b] Key Laboratory of Eco-hydrology of Inland River Basin, Northwest Institute of Eco-Environment and Resources, Chinese Academy of Sciences, Lanzhou 730000, China

[c] Centre for Ecosystem Science, School of Biological, Earth and Environmental Sciences, University of New South Wales, Kensington 2052 NSW, Australia

[d] Laboratory of Basin Hydrology and Wetland Eco-restoration, China University of Geosciences, Wuhan 430074, China

[e] School of Life Science, University of Technology Sydney, Ultimo 2007 NSW, Australia

*Correspondence to lzxhhs@163.com (Zongxing Li); Daniel.Ramp@uts.edu.au (Daniel Ramp)

Abstract

This research developed a method of tracing major water chemical parameters (WCP) and soil heavy metals (HM) to identify the processes of mining pollution in topographically complex landscapes. Ninety-nine spatially distributed water samples were collected to characterise the hydrochemical characteristics of an alpine river in north-west China. Sixty river WCP and fifty-six soil HM samples from areas near mining sites were then used to analyse the mining pollution process. Geographical and mining activity characteristics were derived from topographic and mine site information. The occurrence of sulphates (SO_4^{2-}) and nitrates (NO_3^-) in river water were highly correlated (up to 0.70), providing strong evidence of pollution from nearby mining activities. Levels of arsenic and cadmium were high in first and fifth order streams, where mining activities were most concentrated. The modelling results showed that geographical patterns and mining activity account for predicting HM distribution, and WCP can be reasonable predictors to trace soil mining pollution. This research can help improve the accuracy of predicting the mining pollution process.

Key words: alpine catchment, mining activity, soil heavy metals, water chemical parameters, geographical characteristics, stream orders, generalised additive models

1. Introduction

Water resources are essential for supporting humans and ecosystems, making water availability and security a challenging global problem of great importance (Tilman et al., 2002; Vörösmarty et al., 2010). Water quantity and quality are two widely used criteria for evaluating water resource levels, both of which are highly sensitive to human activity (Novotny, 2003; Scanlon et al., 2007). Deterioration in water quality can occur as a direct or indirect response to pollution, which conveys negative contaminants into aquatic systems and alters chemical composition, bacterial and nutrient accumulation, and sediment transport (Hounslow, 2018). Rapid economic growth over recent decades has necessitated greater levels of mineral exploitation, required to provide important elements needed for developing populations (Duarte et al., 2019; Gredilla et al., 2019; Oliveira et al., 2019). However, mining activities typically require large quantities of water to process ore (Gunson et al., 2012), resulting in occurrences of mine effluent discharge and tailings seepage (Ramos et al., 2017; Nordin et al., 2018; Sánchez-Peña et al., 2018). This can lead to serious contamination of freshwater resources and polluted wastewater must often be managed for decades (Candeias et al., 2015; Fetter et al., 2017). Mining pollutants can drain directly into local runoff over land or can be dispersed into rivers via rainfall or other hydrological processes (Oliveira et al., 2018; Sánchez-Peña et al., 2018). Pollutants that infiltrate deep soil or enter streams can be transported into aquifers by exchange processes between ground and surface water. Groundwater can also be polluted directly if the aquifer system is destroyed through mining activity (Armienta and Segovia, 2008). Although the effect of mining on water quality has been well studied on river areas proximal to mining activities in low altitude environments (Kondolf, 1997), the process of large scale mining impacts within alpine catchments is more complicated and less studied. For example, mountainous geomorphology can significantly alter the export of weathering solutes and

transport pathways (Rascher et al., 2018; Wellen et al., 2018). Furthermore, alpine topographic features make it more difficult to understand transport processes of contaminants in upstream environments.

The upper reaches of alpine catchments are the powerhouse of freshwater generation and play an important role in enabling ecological balance and agricultural production in the middle and lower reaches (Gredilla et al., 2019). Runoff in these catchments is heavily influenced by changing climate conditions and extreme weather events (Arnell, 2003; Painter et al., 2010; Li et al., 2016). However, because valuable mineral resources are often located in mountainous locations, mining activities frequently occur in these locations, compounding other anthropogenic effects (Nordin et al., 2018; Sánchez-Peña et al., 2018). Traditionally, heavy metals (HM) are used to trace pollutants in the soil (Kabata-Pendias, 2010), atmosphere (Francová et al., 2017), and aquatic systems (Tiwari et al., 2015; Tiwary et al., 2018). HM are often traced directly without considering conversion forces, and previous research has primarily focussed on each of these transmission media separately. However, combining these forces can help to understand the mechanisms that result in movement and exchange between them (Borrok et al., 2009). To provide a more holistic view of HM pollution, one solution is to examine a range of hydrochemical characteristics, as they are well suited to mapping hydrological processes (Adams et al., 2001) and pollutants from anthropogenic activities (Jalali, 2007). This is because water chemical parameters (WCP) can trace sources of river water components (Helena et al., 2000), incorporating exchanges among soil, rock, and air, as well as from additional sources (e.g. from human activity). Water ions (Ca^{2+}, Mg^{2+}, SO_4^{2-}, NO_3^-, etc.) and other physicochemical parameters, such as pH, electric conductivity (EC), and total dissolved solids (TDS), are important WCP that can be used to trace HM pollution, particularly for characterising water-rock interactions (Wellen et al., 2018). Therefore, improvements in

understanding mining pollution may be gained by examining the interaction of WCP with trace elements from other carriers, such as soil HM within the environment.

In this study, samples of river water and soil from an alpine catchment in northwest China were analysed to consider two areas of interest. First, we characterised and traced hydrochemical characteristics in the rivers, groundwater, melt, and precipitation within the catchment. Second, we used modelling techniques to predict the dispersal of soil HM from mining activities across the alpine catchment by quantifying the geographic variations and mining intensity information. This research highlights the correlation between the WCP and soil HM to interpret the process of mining pollution.

2. Methods and dataset

2.1 Study area

This study focused on the upper reaches of the Heihe River, China, as it is a topographically complex alpine landscape with a long mining history (Wei et al., 2018). The Heihe River has a length of 812 km, originating in the snow and glaciers of the Qilian Mountains in the north-eastern of the Qinghai–Tibet Plateau, flowing into the Zhangye Basin through the Yingluoxia hydrological station, and finally entering the Ejinaqi oasis (Fig. 1a). As the river traverses down from the plateau, beginning from glaciers above 4500 m asl, perennial snow persists above 4000 m asl while forests begin from elevations below 3000 m asl. The mean annual temperature in the upper reaches is between −3 and 4°C. The river region experiences a four-month wet season, occurring from June to September, during which more than seventy percent of annual precipitation occurs. Runoff from the upper reaches is the main source of flow generation, with an outbound runoff volume of 2.475×10^9 m^3 annually, directly influencing water availability in the middle and lower reaches (Tian et al., 2018). The area is characterised by steep mountain

valleys, with marked vertical zonations of vegetation, including glacier, alpine cold desert, marsh meadow, alpine shrub, and mountain grassland (Wang et al., 2009). The Zhamashike River (ZMSK) is the western branch of the upper stream, has a catchment area of approximately 5512 km^2 and an average elevation of 3929 m (Fig. 1b). Flow variation in the ZMSK is distinctly seasonal, with 44.43 × 10^4 m^3/day flow in summer, but only 6.06 × 10^4 m^3/day flow in winter.

Geologically, the Hiehe catchment is situated in the northern Qilian orogenic belt, between the Qilian and Alashan Blocks. The belt is an oceanic suture composed of subduction accretionary complexes. The ZMSK flows NW-SE through post-Devonian sedimentary cover, Quaternary cover, island arc volcanic rocks, and granites (Fig. 1c). Other covers include Neoproterozoic to early Paleozoic ophiolite sequences, and high-pressure metamorphic rocks. The primary metallogenic period of the area is early Paleozoic, while the lithology is composed of epi-metamorphic rock series, including clasolites, extrusive rocks, carbonates, and igneous rocks (Wei et al., 2018).

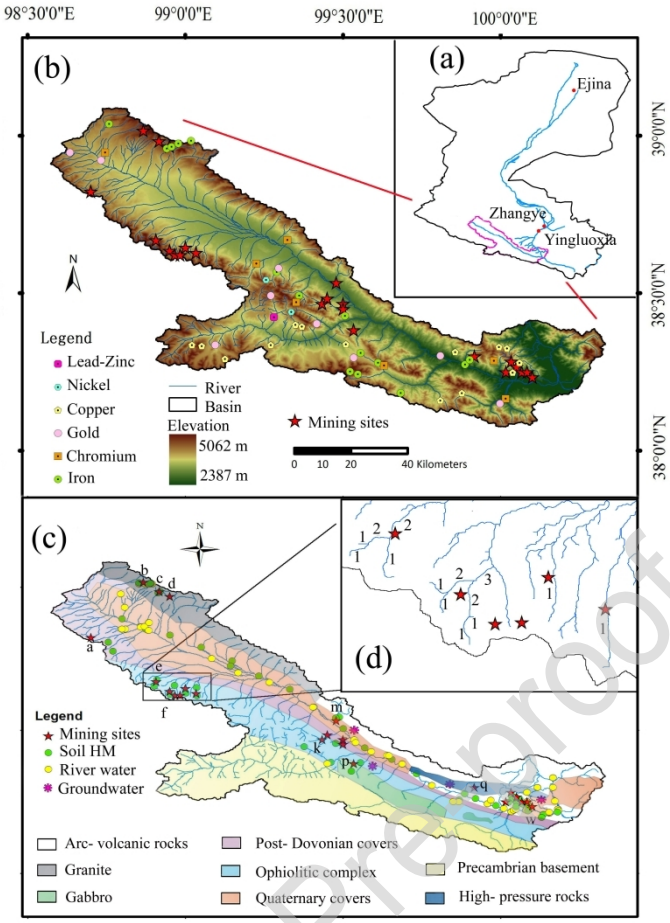

Fig. 1. Study site showing: (a) ZMSK in the Heihe River catchment (pink boundary line); and (b) location of known mineral deposits and mining sites; (c) soil and water sampling sites, lithology (adapted from Wei et al., 2018), and mining sites ID (following a longitude sequence from "a" to "w"); and (d) stream order systems.

The region is rich in mineral resources, including coal, copper, lead, and zinc (Fig. 1b). Consequently, the study area has an extensive mining history over last four decades (Wei et al., 2018), with 23 mining sites possessing government licences during our survey in August 2013 (Table 1).

Table 1. Detailed information for mining sites in the study catchment. The mine sites from "a" to "j" are considered in the upper part of the catchment, and almost of them are open pit

mining. The “k” to “p” are in the middle part, and “l” to “w” are in the outlet part. OP: open pit mining; UG: underground mining (adapted from Wei et al., 2018)

ID	Extracted volume (10^4 t/year)	Status	Extraction method	Upper limit line (m asl)	Lower limit line (m asl)	Depth (m)	Area(km^2)	Wastes deposited volume (m^3)	Permission time range	Lithology
a	0.15	Abandoned	OP	4290	4190	100	0.57	84530	07/2010-12/2014	Precambrian
b	0.33	Abandoned	OP	4582	4280	302	0.09	-	01/2013-01/2016	Granite
c	-	Completed	OP	4600	4300	300	0.50	22001	12/2010-08/2013	Granite
d	28.33	Active	UG	4745	4240	505	1.12	-	11/2010-11/2013	Granite
e	1.30	Abandoned	OP	4308	4238	70	0.11	-	06/2011-07/2014	Mantle peridotite
f	3.06	Active	OP	4630	4362	268	1.30	83260	07/2012-07/2017	Gabbro
g	0.35	Active	UG	4560	4280	280	0.31	22003	07/2012-07/2013	Gabbro
h	1.25	Abandoned	UG	4539	4360	179	0.06	-	08/2011-08/2015	Gabbro
i	1.30	Active	OP	4330	4200	130	0.07	85500	06/2011-07/2014	Gabbro
j	1.30	Abandoned	OP	4290	4220	70	0.03	-	06/2011-07/2014	Gabbro
k	5.25	Completed	Both	4460	4020	440	0.52	33000	03/2010-10/2013	Post-Dovonian
l	-	Completed	UG	3959	3520	439	0.52	22001	12/2010-10/2013	Post-Dovonian
m	3.25	Completed	UG	3650	3620	30	0.11	-	06/2011-06/2014	Quaternary covers
n	-	Completed	UG	3959	3520	439	0.52	-	12/2010-10/2013	Post-Dovonian
o	-	Completed	UG	3959	3520	439	0.52	-	12/2010-10/2013	Post-Dovonian
p	0.50	Abandoned	UG	4100	3920	180	0.12	32007	12/2011-06/2014	Post-Dovonian
q	0.58	Active	UG	3130	3018	112	0.16	27002	07/2012-07/2015	Arc-volcanic rocks
r	1.67	Completed	UG	3530	3000	530	0.13	37007	10/2012-10/2013	Arc-volcanic rocks

s	10.67	Active	Both	3680	3150	530	0.54	-	12/2010-07/2013	Arc-volcanic rocks
t	6.50	Completed	UG	3460	3084	376	0.12	-	06/2011-06/2013	Arc-volcanic rocks
u	4.50	Completed	UG	3150	2790	360	0.19	-	03/2012-10/2015	Arc-volcanic rocks
v	8.00	Abandoned	UG	3159	2730	429	0.20	-	12/2010-01/2013	Arc-volcanic rocks
w	-	Active	UG	2694	2550	144	1.07	-	07/2011-09/2013	Arc-volcanic rocks

2.2 Water and soil sampling

Ninety-nine water samples were collected between June 2012 and August 2013 across an elevation range of 2586–4740 m asl, comprising samples from rivers, wells, springs, precipitation, and meltwater from glaciers and snow (Fig. 1c). Sixty river samples (40 during summer, 20 during winter) were collected from the glacier terminus to the outlet along the main river channel. Thirteen groundwater samples were collected, five from deep wells and eight from exposed springs. Eight glacier–snow meltwater samples were collected at the terminus of the Shiyi glacier during the ablation period. Eighteen precipitation samples were collected, one for each precipitation event that occurred at Shiyi glacier station. All samples were stored at 4°C prior to laboratory analysis. The geochemical composition of all samples was analysed using a Dionex-600 Ion Chromatograph (IC), while anions were analysed using a Dionex-2500 IC. Analytical precision was 95.6% for Ca^{2+}, 103.7% for Mg^{2+}, 94.3% for Na^{+}, 96.8% for K^{+}, and 98.6% for SO_4^{2-}, 97.2% for Cl^{-} and 96.4% for NO_3^{-}.

We used fifty-six surface soil samples from a previous study (Bu et al., 2016), collected adjacent to mining sites in the catchment during August 2013 (Fig. 1c). A clean plastic dustpan and brush were used to collect samples from the top 20 cm of soil and each sample was stored

in a plastic bag. All soil samples were air dried and kept at 20°C until analysis. HM concentrations were measured using inductively coupled plasma mass spectrometry (ICP-MS). Sampling and analytical procedures followed previously published methodologies for tracing mining pollution and activity (Sanchís et al., 2015; Civeira et al., 2016a,b; Rodriguez-Iruretagoiena et al., 2016).

2.3 Stream order system

To understand variation in water pollutant concentration contributed to by mining activity across different stream scales, stream position and order was defined by the numerical order of branches in the river system (Horton, 1945; Strahler, 1957). Different methods for topologically ordering tributaries according to their distance from primary sources are available, however, we chose the Strahler method as it assigns the outermost tributaries as 'first order', making it valuable for analysing headwater quality (Scheidegger, 1965; Kang et al., 2008). Stream order increases when two streams of the same order merge. Where two links of different orders intersect, the higher of the two orders is given. Stream order was analysed using ArcGIS 10.5 (Environmental Systems Research Institute Inc.), using a 30 m resolution digital elevation model (DEM). Using the hydrology toolset in ArcMap 10.5, outlets were identified and then catchments and sinks extracted from the DEM, as well as flow direction and accumulation. An area of 10 hectares was applied as the 'minimum accumulation area' to create streams and outlets for the stream order network.

During summer sampling, nine river samples were from first-order streams, six samples from second, third and fourth-order streams, and thirteen from fifth-order streams (Fig. 1d, Table 2). During winter, four river samples were from first and second-order streams, two from third-order streams, three from fourth-order streams, and seven from fifth-order streams. There were twenty-two, eleven, five, four, and fourteen soil HM samples adjacent to first to fifth-order

streams. Of the twenty-three authorised mining sites, nine were adjacent to first-order streams, one was proximal to a second-order stream, while the remaining thirteen were all adjacent to fifth-order streams.

Table 2. The number of water samples, soil samples, and mining sites in or adjacent to different stream orders (first to fifth).

Orders	Stream summer	Stream winter	Soil samplings	Mining
First	9	4	22	9
Second	6	4	11	1
Third	6	2	5	0
Fourth	6	3	4	0
Fifth	13	7	14	13

2.4 Predicting heavy metal distributions

The regional distributions of HM were obtained by modelling the spatial patterning of HM from terrain and mining activity. The geographic complexity of the alpine catchment was captured by calculating topographic variation within the DEM using the 'terrain' function in the 'raster' package in R v3.5.1 (R Core Team 2018): slope, aspect, flow direction, TRI (Terrain Ruggedness Index), TPI (Topographic Position Index), and roughness. TRI is the difference between the absolute elevation values of a cell and the values of its eight encompassing cells. TPI is calculated as the difference between the value of a cell and the mean value of its eight surrounding cells. Roughness is used to show the difference between the highest and the lowest cell values and its eight encompassing cells.

To account for variation attributed to the proximity and intensity of mining activities, we calculated two spatial functions from mine site locations, mine density and distance to the nearest mine (m). The function 'bkde2D' in R was used to perform a two-dimensional kernel density estimation of mining activity, using a bandwidth of 0.05. Distance to the nearest mine was obtained using the function of 'distanceFromPoints', calculating the distance from a group of points to sampling points. Generalised linear models (glm) were run for each HM variable using topographic variables, elevation (m), slope (degrees), TPI, TRI, and roughness, and the two mine activity variables in R, using the 'mgcv' package. The 'predict' function was then used to create rasters of the predicted HM distribution across the entire catchment.

2.5 Tracing heavy metals through water chemistry parameters

To interpolate values of HM to water sampling sites, we extracted raster values at all locations, using the 'extract' function in the 'raster' package in R. Generalised additive models (gam) were then used to model the relationship between HM and WCP using the 'mgcv' package to account for potential non-linear relationships. K^+, Na^+, TDS, and total ions were removed due to high correlation with other parameters (>0.7). Model selection was employed to identify the best candidate model from a combination of all possible models. Using model averaging approaches in the 'MuMIn' package in R, models were ranked in order of importance based on the Akaike information criterion (AIC) and those variables included in the best model set (AIC < 2) were used to find the best model for each HM.

3. Results

3.1 Hydrological background valuesv

The total dissolved solids (TDS) in the river water ranged from 134.48 to 711.76 mg L^{-1}, with a mean value of 367.42 mg L^{-1} (Table 3); this is more than three times the global average TDS

for river water (115 mg L^{-1}; Zhu and Yang, 2007). Well water had the highest mean TDS (489.8 mg L^{-1}). The highest mean electric conductivity (EC) was in meltwater (1074.75 μS cm^{-1}), followed by water from wells, springs, rivers, and precipitation (Table 3). The mean EC value for river water was 600.93 μS cm^{-1}, ranging from 244.5 to 1148 μS cm^{-1}. The rank order of cations in the river water, from highest to lowest concentration, was Ca^{2+}＞Mg^{2+}＞Na^{+}＞K^{+}. The rank order for anions, from highest to lowest concentration, was SO_4^{2-} ＞Cl^{-}＞NO_3^{-}. SO_4^{2-}, Ca^{2+} and Mg^{2+} were the ions with highest concentration in river water, accounting for 45.8%, 27.2% and 10.4% of the total ionic concentration respectively. The water from the river, springs, wells, and meltwater was of the SO_4^{2-}–Mg^{2+}–Ca^{2+} type, with these ions accounting for more than 80% of the total ionic concentrations (Fig. 2). There were seasonal patterns evident, with the concentrations of most river water samples from winter being higher than those from summer. The mean values of Mg^{2+}， Na^{+}， K^{+}， NO_3^{-}， SO_4^{2-} in river water in winter were 35.81, 22.66, 2.28, 21.88 and 160.27 mg L^{-1} respectively, whereas the mean values of those ions in summer were 23.31, 11.41, 1.83, 7.40 and 102.14 mg L^{-1} respectively.

Table 3. Average ionic composition (mg L^{-1}) of different water types from ZMSK.

Samples	EC (μS cm^{-1})	TDS (mg L^{-1})	pH	Ca^{2+}	Mg^{2+}	Na^{+}	K^{+}	NO_3^{-}	SO_4^{2-}	Cl^{-}
River	600.93	367.42	8.08	71.91	27.47	15.16	1.98	12.22	121.52	14.85
max	1148.00	711.76	9.14	110.96	43.28	32.09	2.75	37.94	317.18	43.55
min	244.50	134.48	7.14	47.45	9.12	6.99	0.82	0.21	8.76	4.00
Spring	707.75	461.83	7.85	83.69	34.64	16.14	2.06	23.34	173.96	17.51
Well	788.00	489.80	7.74	99.81	56.79	55.15	5.32	65.28	193.92	44.57
Meltwater	1074.75	402.02	7.99	208.87	41.34	97.84	5.89	4.93	463.30	30.09
Precipitation	14.51	7.85	7.54	17.39	3.31	5.91	2.31	4.23	8.26	3.38
WHO limits	1500	-	6.5-8.5	200	150	200	-	-	-	250

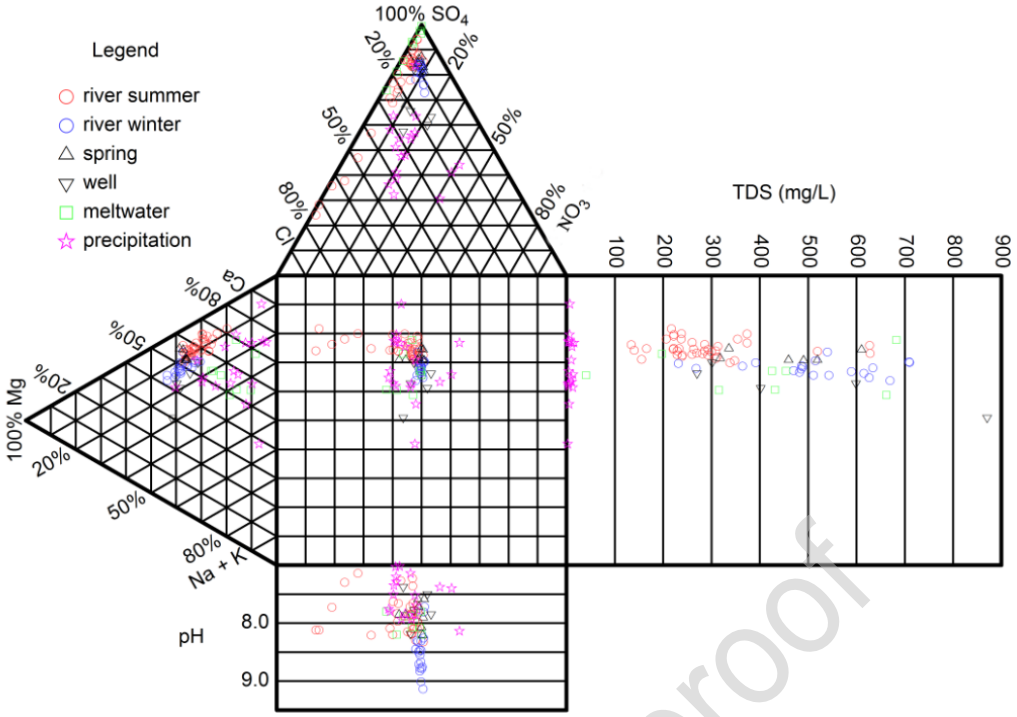

Fig. 2. Durov plot to graphically show cation and anion concentrations, pH, and TDS of the multiple water samples. The water sample points in the square grid are projected onto two separate triangular plots to depict the percentage values of cations and anions, and onto two rectangle plots to show the pH and TDS separately.

The ionic concentrations of water samples in the ZMSK met all the requirements for drinking water according to World Health Organisation (WHO) standards (Lin et al., 2012). Water samples also met most of China's Environmental Quality Standards in GB383-2002 for surface water and GB/T 14848-93 for groundwater (Han et al., 2016). All waters were alkaline, with pH values greater than 7.0 (Fig. 2). The pH value of river water in summer ranged from 7.14 to 8.33, with an average value of 7.87; this was lower than that of river water in winter, which ranged from 7.72 to 9.14, with an average of 8.5. Under the drinking water standards, pH values should be between 6.5 and 8.5. All summer samples were within this range and 10 of the 20 winter samples were above the range. The processes controlling stream solute chemistry are complicated (Kim et al., 2017), and the recharge sources may explain the higher pH in winter.

This catchment is mainly recharged by wet precipitation in summer with a lower pH (Zhao et al., 2011), while in winter the groundwater with a high pH plays a more important role. Further research is needed for specific mechanism.

3.2 Water chemical composition sources

Although the study area has been influenced by other human activities, the main anthropogenic pollutants were expected to be from mining, with the contribution from other activities likely to be negligible. To test this hypothesis, a Pearson correlation analysis was applied to study the relationships between ions, TDS, EC, and pH, and to identify possible sources. Considering the temporal variations in the water chemical composition, separate analyses were undertaken for river water in seasons. When the correlation coefficient between two elements is over 0.5, it is assumed that they have the communal possible sources. Shapiro-Wilk test was applied to examine the normality. Due to the p values of Na^+, TDS and pH in river water during summer were 0.001, 0.000 and 0.02, they were removed for the Pearson correlation analysis. In summer, there were significant positive correlations between SO_4^{2-} and all other components except Cl^- (Table 4). SO_4^{2-} and Ca^{2+} were the ions with the highest concentration in the river water in summer, and the significant correlation between them indicated the contribution of gypsum to the composition of the river water. Nitrates (NO_3^-) usually indicate a human influence (Mayer et al., 2002), such as fuel burning by large machinery. NO_3^- was significantly correlated with most ions, especially Ca^{2+}, Mg^{2+}, Na^{2+}, SO_4^{2-} and K^+ (Table 4).

Table 4. Pearson correlation analysis (r values) of ions taken from river water during summer (left below) and winter (right top).

Summer Winter	Ca^{2+}	Mg^{2+}	Na^+	K^+	NO_3^-	SO_4^{2-}	Cl^-	TDS	EC	pH
Ca^{2+}	1	0.242	**0.521***	**0.661***	**0.823***	**0.673***	0.497	0.293	0.301	−0.678
Mg^{2+}	**0.815***	1	0.373	**0.542***	**0.512***	**0.683***	**0.803***	**0.708***	**0.698***	−0.007

Na^+	-	-	1	**0.883***	0.401	−0.197	0.293	0.471	0.503	−0.236
K^+	**0.500***	**0.789***	-	1	0.433	0.09	**0.577***	**0.536***	**0.548***	−0.447
NO_3^-	**0.773***	**0.713***	-	**0.675***	1	0.084	**0.718***	0.494	**0.503***	−0.678
SO_4^{2-}	**0.753***	**0.834***	-	**0.688***	**0.700***	1	**0.568***	0.412	0.373	0.09
Cl^-	0.428	0.065	-	−0.256	0.205	0.095	1	**0.562***	**0.552***	−0.496
TDS	-	-	-	-	-	-	-	1	**0.997***	−0.104
EC	0.45	0.376	-	0.273	0.495	**0.530***	0.122	-	1	−0.096
pH	-	-	-	-	-	-	-	-	-	1

In the winter water samples (Table 4), SO_4^{2-} was significantly positively correlated with Ca^{2+} and Mg^{2+}, indicating the contributions of $CaSO_4$ and $MgSO_4$ dissolution to runoff. The correlations were less strong than in those from the summer samples, indicating that the weathering intensity of rock is weaker in winter. In addition, SO_4^{2-} was not significantly correlated with NO_3^- or K^+ in winter, which contrasts with strong correlations in summer. This was associated with less mining activity during winter, and the seasonal variation of river flow from summer to winter may also play an important role. NO_3^- was strongly positively correlated with Ca^{2+}, Mg^{2+} and Cl^-; however, NO_3^- was not correlated with SO_4^{2-}, Cl^- or K^+ in winter, which again contrasts with strong correlations in summer. Finally, Mg^{2+} and Ca^{2+} were not significantly correlated in winter, but they were positively correlated in summer (Table 4).

3.3 Stream order system

First-order streams usually have wide riparian buffers that provide convenience for human activity. There are also no recharge sources from upstream, making them a good index to trace nonpoint source pollution. The median values of sulfates in summer did not show any variation trends, but rather showed higher individual values at the first and fifth-order streams (Fig. 3a). A similar distribution was observed for nitrates in summer (Fig. 3b). The high sulphate and nitrate concentrations in surface water and groundwater were likely caused by mining and

agricultural activity (Rivett et al., 2008; Mativenga and Marnewick, 2018). Agriculture is limited in this location due to the cold weather and complicated landform (Gao et al., 2013). Thirteen mining sites in the alpine catchment were distributed near the main stream areas, where the elevation is lower and accessibility is greater for mining operations and transportation. This may explain the high concentrations of sulfates and nitrates in the last order streams. In contrast, most other mining points were distributed near the first-order streams. These areas were originally covered by bare rocks with low plant cover, which was more convenient for mining exploitation. The high levels of pollutants in the original area also correlated with the level of mining activity.

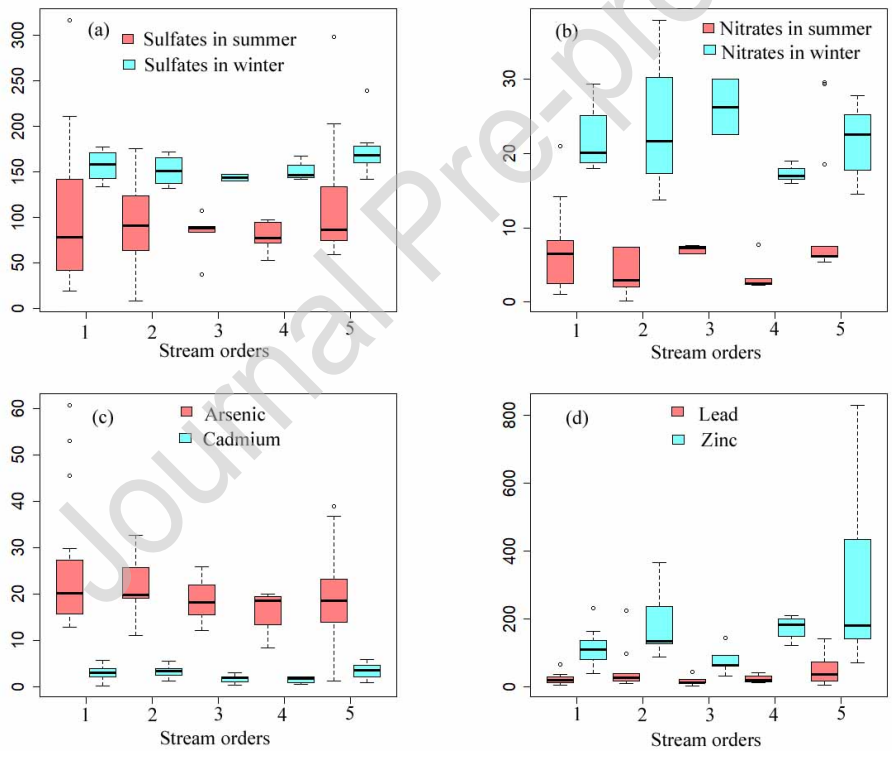

Fig. 3. Sulphates, nitrates, and soil HM concentrations in relation to stream orders in the ZMSK, and the units for sulfates and nitrates are mg L^{-1}, for HMs being mg kg^{-1}.

The areas in which mining activity occurs have the highest concentrations of sulfates and nitrates, and other stream order systems have lower pollutant concentrations. Adverse natural

conditions make mining activities more difficult in winter, so the distribution of sulfates and nitrates in winter did not show any obvious trend (Fig. 3a and Fig. 3b). Regarding soil HM, the concentrations of As and Cd were highest in the first and fifth-order streams (Fig. 3c), while high concentrations of Pb and Zn were only found near the main stream areas (Fig. 3d).

3.4 Predicted dispersal of heavy metals

The dispersal of the HM contaminants from mine sites were predicted from geographical characteristics and mining activity characteristics (Fig. 4). HM values around mining sites were naturally highest, with most mining in the upper catchment centred around headwater areas. HM concentrations decreased from these headwater regions down to the main stream, reflecting attenuation processes over space. The prevalence of mining pollution in mountainous catchments is strongly driven by topography, stream dynamics, and land use. Compared to simple spatial interpolation in this area (Bu et al., 2016; Wei et al., 2018), predicted HM distributions can better reflect transport of mining pollution when using complex topographic information to address geospatial patterns.

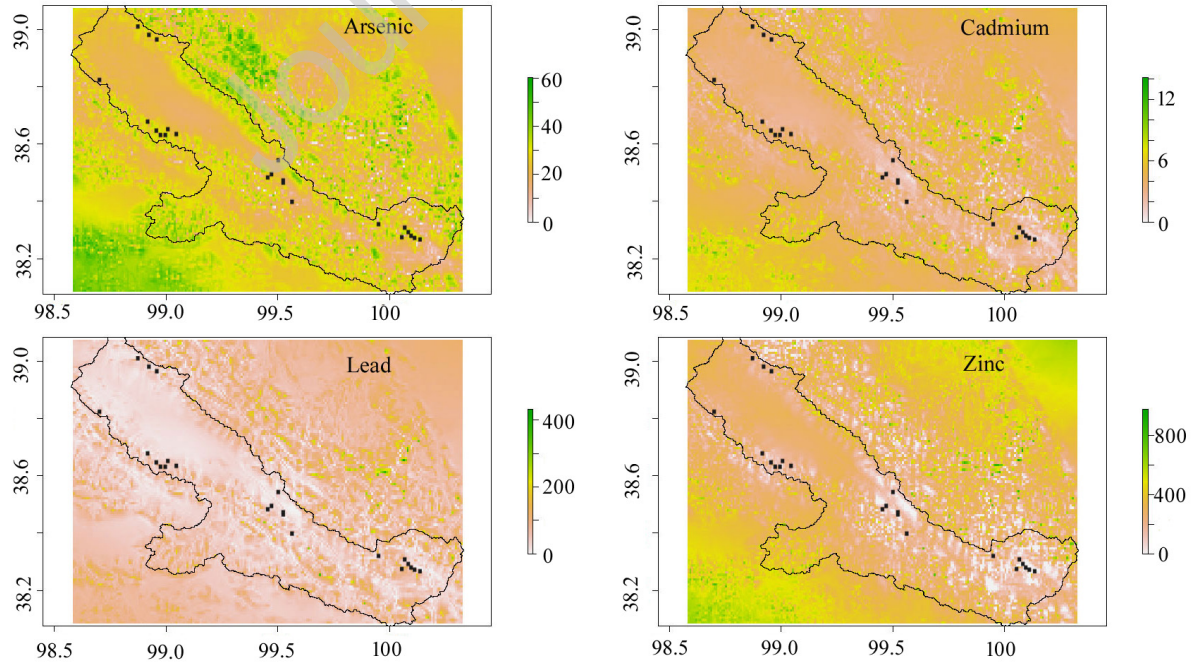

Fig. 4. The predicted spatial dispersal of HM (mg kg^{-1}) in the ZMSK.

3.5 Tracing heavy metals

Model selection identified the top models from all combinations of WCP for each HM. Models with the lowest AICc are listed in Table 5, highlighting the included variables and model support relative to other models within 2 AICc. When EC, NO_3^- and pH were selected as the smoothed variables, the AICc value of the top model for tracing arsenic was 322.34, and the degrees of freedom (df) was 13 (Table 5). The pH was also a smoothed variable in the top model for tracing cadmium and zinc. The top model for tracing lead was dominant by NO_3^- and SO_4^{2-}, and the AICc value was 526.19.

Table 5. Top models identified through model selection based on AICc.

Heavy metal	Smoothed variables in best model	Degrees of freedom (df)	loglik	AICc	Akaike weight
Arsenic	EC + NO_3^- + pH	13	-142.74	322.34	0.6
Cadmium	Ca^{2+} + pH	6	-76	166.16	0.6
Lead	NO_3^- + SO_4^{2-}	7	-254.45	526.19	0.45
Zinc	pH + SO_4^{2-}	4	-352.01	712.75	0.17

Additional variables were included in models also within 2AICc of the best model. To not discount their influence on HM, these additional variables, where appropriate, were included in final models for each HM (Table 6). The final model for arsenic kept the same three variables as the top model, and the deviance explained (DE) value of these variables was 51.4%. The concentration of arsenic fluctuated in relation to NO_3^- concentration, reaching the minimum value when the concentration of NO_3^- was around 6 mg L^{-1}, and showed a constant trend when

the NO_3^- concentration was higher than 28 mg L^{-1} (Fig. 5a). Arsenic also showed a nonlinear relationship with pH, and increasing when pH was below 8.3, but decreasing after this point (Fig. 5b).

Both NO_3^- and pH were also smoothed variables for the other three HM, but showed the opposite trend. The NO_3^- displayed negative linear relationship with the concentrations of cadmium and zinc (Fig. 5f, 5l), while there was a positive linear relationship with lead (Fig. 5h). Conversely, pH was correlated with cadmium and zinc (Fig. 5d, 5n), but displayed negative linear relationship with lead (Fig. 5j).

Table 6. Generalised Additive Models (gam) describing the response of heavy metals (HM) to major water chemical parameters (WCP).

Heavy Metals	Variable	Degrees of freedom estimated to model(Edf)	Degrees of freedom estimated to waste (Ref.df)	Significance of smoothed terms (F)	P-value	Deviance explained (DE)
Arsenic	NO_3^-	8.738	8.977	3.394	0.001	51.4%
	pH	2.124	2.654	1.991	0.153	
	EC	1	1	4.867	0.032	
Cadmium	pH	1	1	5.102	0.028	20.5%
	Ca^{2+}	3.122	3.92	1.832	0.119	
	NO_3^-	1	1	0.303	0.584	
Lead	SO_4^{2-}	4.088	4.938	1.559	0.188	26.8%
	NO_3^-	1	1	2.76	0.103	
	Ca^{2+}	1	1	0.127	0.723	
	pH	1	1	1.012	0.319	
Zinc	SO_4^{2-}	5.395	6.446	0.951	0.405	26.3%

NO_3^-	1	1	2.691	0.107
Ca^{2+}	1.741	2.224	0.438	0.776
pH	1	1	0.599	0.443
Mg^{2+}	1	1	1.364	0.249
EC	1	1	0.432	0.514

The concentrations of lead decreased when the SO_4^{2-} concentration was less than 140 mg L^{-1}, kept increasing after that point until the SO_4^{2-} concentration was around 240 mg L^{-1}, and then decreased again (Fig. 5g). Compared to the top model for tracing zinc, the smoothed variables of NO_3^-, Ca^{2+}, Mg^{2+} and EC remained within 2AICc of the best model (Table 6). The concentrations of zinc fluctuated with SO_4^{2-} concentration, and two low peaks were reached when SO_4^{2-} concentration was 100 and 255 mg L^{-1} (Fig. 5k). The Mg^{2+} and EC showed positive linear relationship with zinc (Fig. 5o, 5p), while there was no significant change with Ca^{2+} (Fig. 5m). Zinc kept decreasing slightly, but remained constant when the Ca^{2+} concentration was over 70 mg L^{-1}.

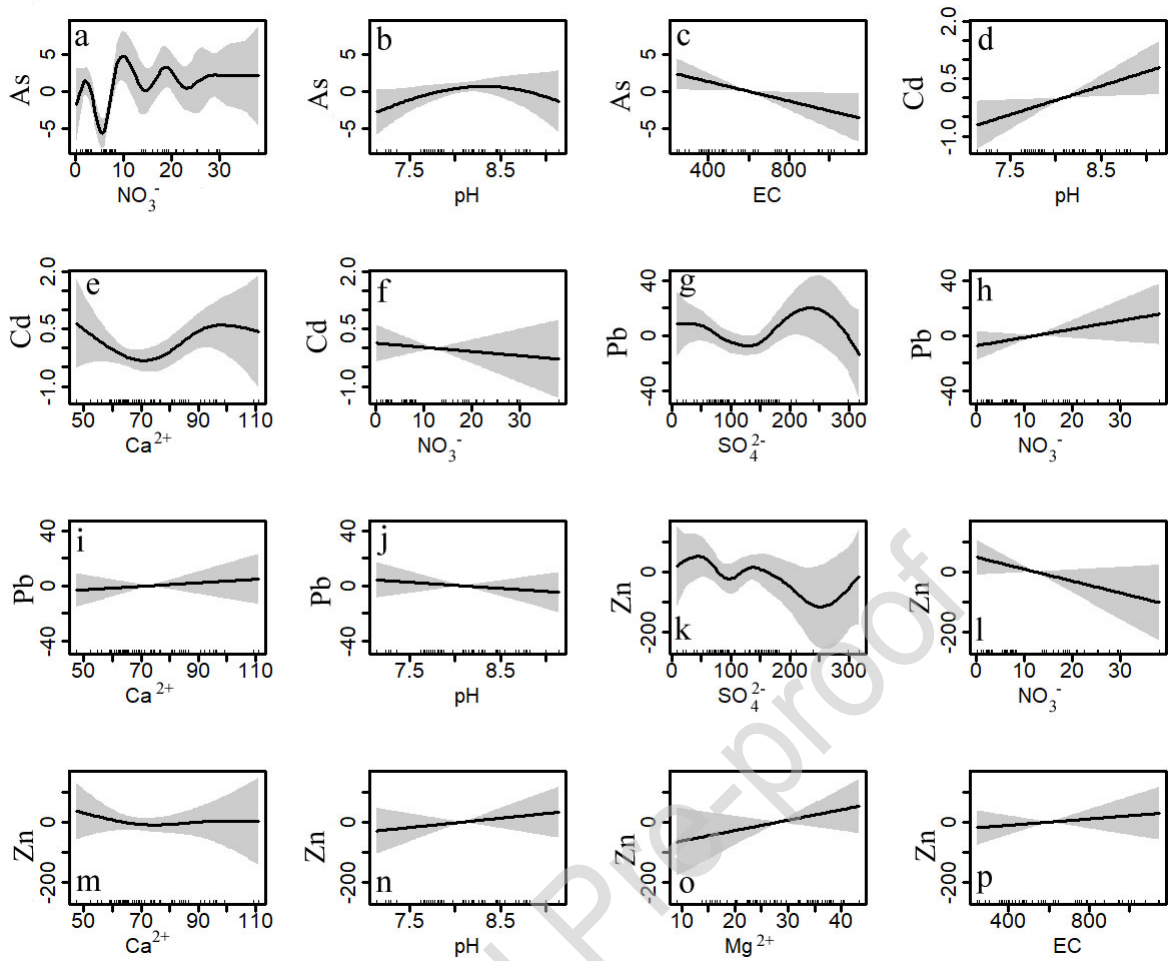

Fig. 5. Smoothed fits of relationships between WCP and HM. Tick marks on the x-axis are observed data points. The y-axis stands for the As (a to c), Cd (d to f), Pb (g to j), Zn (k to p).

4. Discussion

4.1 The possibility of water chemical parameters to trace mining activity

Chemical analysis of the main stream water met the standards for drinking and irrigation standards in the ZMSK, but previous research has found that tributaries were affected by local mining activity (Wei et al., 2018). Effective control of anthropogenic pollution here is crucial. The nitrate in river catchments is a common nitrogenous compound from the nitrogen cycle,

but anthropogenic sources have greatly increased the concentration level, including discharges from fertilized agricultural lands (Matson et al., 1997), industrial waste water (Abdel-Halim et al., 2003), landfills, and energy consumption (Li et al., 2017). However, NO_3^- in the catchment was significantly positively correlated with most of other parameters during summer, reflecting the influence of human activities, such as energy consumption from mining operation equipment and vehicle emission from mining transportation. The NO_3^- here almost from the anthropogenic activity was further supported by the small content of NO_3^- in the river water.

Sulfates in river water are often formed as the result of the water passing through rock or soil containing gypsum and other common minerals, or atmospheric deposition (Azabou et al., 2007; Shaffer et al., 2017). The high contents of SO_4^{2-} in river water showed the abundance of sulfide deposits in the catchment (Ma et al., 2009). Point sources, such as treatment and industrial discharges, and agricultural lands also contribute sulfates to river water (Tüfekci et al., 2007; Smolders et al., 2010). The significant positive correlation between SO_4^{2-} and most of other parameters showed the active activity for sulfates, but it is difficult to identify the natural or anthropogenic contributions. However, the coefficient of correlation between SO_4^{2-} and NO_3^- from the river water was up to 0.70 during summer, while only 0.08 during winter, indicating the human influence from mining activities during the warm periods. This inference was also supported by the stream order system analysis.

Most of the tracing elements, including the HM, have both natural and anthropogenic sources (Plank and Langmuir, 1993; Pacyna and Pacyna, 2001). Combing various tracing elements can give further insight on the contamination mechanism. This study explored to improve the accuracy of predicting the dispersal of soil HM by combining the mining activity and geographical characters. And then modelled the relationship between soil HM and WCP to analyse the mining pollution process. The analysis of WCP is much simpler and relatively

inexpensive than analysing HM, so using the hydrological parameters is also an economic choice.

4.2 Mining pollution mechanism

Geographical characteristics, such as climate and topography parameters, play an important role in the mining pollution at an alpine catchment scale. The precipitation assumption directly determines the runoff volume in a precipitation-recharged catchment (Rodriguez-Iruretagoiena et al., 2016). Topography characteristics effect contamination transmission processes by influencing the stream directions and flow velocity. The soil erosion levels were determined by slopes, aspects, TPI, TRI, roughness and rainfall intensity. Large quantities of rocks are excavated to extract the desired mineral ore during operation at mining sites. The ore is then crushed into finely ground tailings and processed with various chemicals to extract the minerals. During rainfall events, a substantial quantity of sediment can be carried from the mining residuals on steep mountain valleys into the river, the other retained in the soil (Fig. 6).

Apart from natural factors, the variables ‘mining density’ and ‘distance to mining sites’ are necessary to be considered. The results also showed the importance of these two variables. Thus mining pollution in alpine catchment area is a complex process, and more variables should be taken into account when analysing and modelling this process in order to provide more detailed and useful information. Very similar study of gold, coal and other mining results were reported by previous research (Cerqueira et al., 2012; Oliveira et al., 2012; Arenas-Lago et al., 2013; Silva et al., 2013; Cutruneo et al., 2014).

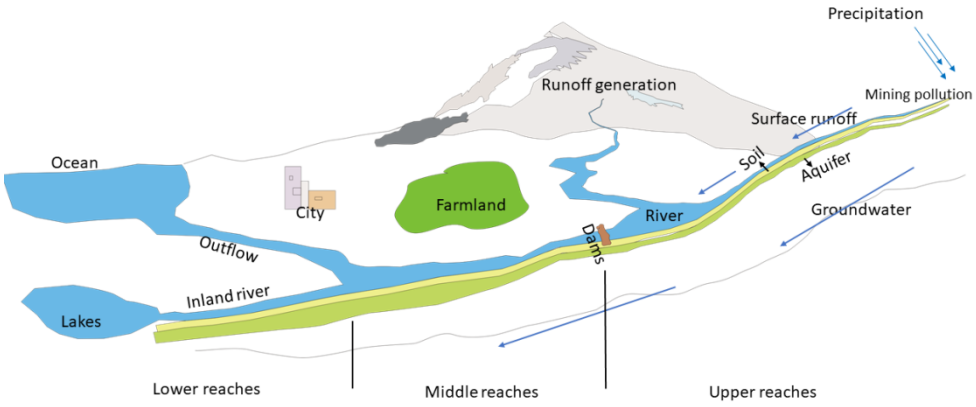

Fig. 6. Conceptual model of mining pollution in alpine catchments.

5. Conclusions

The water from the river, springs, wells, and meltwater spatially distributed in the ZMSK were collected to characterise the hydrochemical characteristics and assess the water quality. Then the WCP and soil HM samples near mining sites were used to analyse the mining pollution process. This research presented a novel method of predicting the dispersal of soil HM by combining geographical factors and mining activity information, and then explored to trace soil HM from WCP around the mining alpine catchment.

The results showed that all water samples were SO_4^{2-}–Mg^{2+}–Ca^{2+} type throughout the year. The strong correlation between SO_4^{2-} and NO_3^- reflected the existing influence of mining activities. The levels of As and Cd were higher in the stream orders where the mining sites were concentrated. The prediction results showed that geographical and mining activity played an important role for the distribution of HM. The model selection results found that NO_3^- and pH were smoothed variables for all these four HM, and WCP are able to be reasonable predictors to trace soil mining pollution.

Increasing sampling density is a necessary method for improving the precision of predicting mining pollution in the future research. We strongly encourage similar research with the interactions between groundwater and surface water, more tracing elements, climate factors and lithology information to provide a more reliable method for analysing mining pollution mechanism at alpine catchments around the world.

Acknowledgments

This study was supported by the Youth Innovation Promotion Association, CAS (2013274), National Nature Science Foundation of China (91547102), National Key R&D Program of China (2017YFC0404305) and the open funding from State Key Laboratory of Urban and Regional Ecology (SKLURE2018-2-6). The first author appreciates the financial support from the Chinese Scholarship Council. He also wants to thank his little daughter Baiyutong (Ruby), Coco and family because he went abroad for a PhD study when the baby was only 2 months old.

References

Abdel-Halim, S., Shehata, A., El-Shahat, M., 2003. Removal of lead ions from industrial waste water by different types of natural materials. Water Research 37, 1678-1683.

Adams, S., Titus, R., Pietersen, K., Tredoux, G., Harris, C., 2001. Hydrochemical characteristics of aquifers near Sutherland in the Western Karoo, South Africa. Journal of Hydrology 241, 91-103.

Arenas-Lago, D., Vega, F., Silva, L., Andrade, M., 2013. Soil interaction and fractionation of added cadmium in some Galician soils. Microchemical Journal 110, 681-690.

Armienta, M., Segovia, N., 2008. Arsenic and fluoride in the groundwater of Mexico. Environmental Geochemistry and Health 30, 345-353.

Arnell, N.W., 2003. Effects of IPCC SRES* emissions scenarios on river runoff: a global perspective. Hydrology and Earth System Sciences Discussions 7, 619-641.

Azabou, S., Mechichi, T., Sayadi, S., 2007. Zinc precipitation by heavy-metal tolerant sulfate-reducing bacteria enriched on phosphogypsum as a sulfate source. Minerals Engineering 20, 173-178.

Borrok, D.M., Wanty, R.B., Ridley, W.I., Lamothe, P.J., Kimball, B.A., Verplanck, P.L., Runkel, R.L., 2009. Application of iron and zinc isotopes to track the sources and mechanisms of metal loading in a mountain watershed. Applied Geochemistry 24, 1270-1277.

Bu, J., Sun, Z., Zhou, A., Xu, Y., Ma, R., Wei, W., Liu, M., 2016. Heavy metals in surface soils in the upper reaches of the Heihe River, northeastern Tibetan Plateau, China. International journal of environmental research and public health 13, 247.

Candeias, C., Ávila, P.F., Da Silva, E.F., Ferreira, A., Durães, N., Teixeira, J.P., 2015. Water–rock interaction and

geochemical processes in surface waters influenced by tailings impoundments: impact and threats to the ecosystems and human health in rural communities (panasqueira mine, central Portugal). Water, Air, & Soil Pollution 226, 23.
Cerqueira, B., Vega, F.A., Silva, L.F., Andrade, L., 2012. Effects of vegetation on chemical and mineralogical characteristics of soils developed on a decantation bank from a copper mine. Science of the Total Environment 421, 220-229.
Civeira, M., Oliveira, M.L., Hower, J.C., Agudelo-Castañeda, D.M., Taffarel, S.R., Ramos, C.G., Kautzmann, R.M., Silva, L.F., 2016a. Modification, adsorption, and geochemistry processes on altered minerals and amorphous phases on the nanometer scale: examples from copper mining refuse, Touro, Spain. Environmental Science and Pollution Research 23, 6535-6545.
Civeira, M., Ramos, C.G., Oliveira, M.L., Kautzmann, R.M., Taffarel, S.R., Teixeira, E.C., Silva, L.F., 2016b. Nano-mineralogy of suspended sediment during the beginning of coal rejects spill. Chemosphere 145, 142-147.
Cutruneo, C.M., Oliveira, M.L., Ward, C.R., Hower, J.C., de Brum, I.A., Sampaio, C.H., Kautzmann, R.M., Taffarel, S.R., Teixeira, E.C., Silva, L.F., 2014. A mineralogical and geochemical study of three Brazilian coal cleaning rejects: demonstration of electron beam applications. International Journal of Coal Geology 130, 33-52.
Duarte, A.L., DaBoit, K., Oliveira, M.L., Teixeira, E.C., Schneider, I.L., Silva, L.F., 2019. Hazardous elements and amorphous nanoparticles in historical estuary coal mining area. Geoscience Frontiers 10, 927-939.
Fetter, C.W., Boving, T., Kreamer, D., 2017. Contaminant hydrogeology. Waveland Press.
Francová, A., Chrastný, V., Šillerová, H., Vítková, M., Kocourková, J., Komárek, M., 2017. Evaluating the suitability of different environmental samples for tracing atmospheric pollution in industrial areas. Environmental Pollution 220, 286-297.
Gao, H., Hrachowitz, M., Fenicia, F., Gharari, S., Savenije, H., 2013. Testing the realism of a topography driven model (FLEX-Topo) in the nested catchments of the Upper Heihe, China. Hydrology & Earth System Sciences Discussions 10.
Gredilla, A., Fdez-Ortiz de Vallejuelo, S, Rodriguez-Iruretagoiena, A., Gómez, L., Oliveira, M.L., Arana, G., De Diego, A., Madariaga, J.M., Silva, L.F., 2019. Evidence of mercury sequestration by carbon nanotubes and nanominerals present in agricultural soils from a coal fired power plant exhaust. Journal of Hazardous Materials, 378, 120747.
Gunson, A., Klein, B., Veiga, M., Dunbar, S., 2012. Reducing mine water requirements. Journal of Cleaner Production 21, 71-82.
Han, D., Currell, M.J., Cao, G., 2016. Deep challenges for China's war on water pollution. Environmental Pollution 218, 1222-1233.
Helena, B., Pardo, R., Vega, M., Barrado, E., Fernandez, J.M., Fernandez, L., 2000. Temporal evolution of groundwater composition in an alluvial aquifer (Pisuerga River, Spain) by principal component analysis. Water Research 34, 807-816.
Horton, R.E., 1945. Erosional development of streams and their drainage basins; hydrophysical approach to quantitative morphology. Geological society of America bulletin 56, 275-370.
Hounslow, A., 2018. Water quality data: analysis and interpretation. CRC press.
Jalali, M., 2007. Hydrochemical identification of groundwater resources and their changes under the impacts of human activity in the Chah basin in western Iran. Environmental Monitoring and Assessment 130, 347-364.
Kabata-Pendias, A., 2010. Trace elements in soils and plants. CRC press.
Kang, S., Lin, H., Gburek, W.J., Folmar, G.J., Lowery, B., 2008. Baseflow nitrate in relation to stream order and agricultural land use. Journal of Environmental Quality 37, 808-816.
Kim, H., Dietrich, W.E., Thurnhoffer, B.M., Bishop, J.K., Fung, I.Y., 2017. Controls on solute concentration - discharge relationships revealed by simultaneous hydrochemistry observations of hillslope runoff and stream flow: The importance of critical zone structure. Water Resources Research 53, 1424-1443.
Kondolf, G.M., 1997. PROFILE: hungry water: effects of dams and gravel mining on river channels. Environmental Management 21, 533-551.
Li, J., Li, Z., Feng, Q., 2017. Impact of anthropogenic and natural processes on the chemical compositions of precipitation at a rapidly urbanized city in Northwest China. Environmental Earth Sciences 76, 380.
Li, Z., Feng, Q., Wang, Q., Song, Y., Li, J., Yongge, L., Yamin, W., 2016. Quantitative evaluation on the influence from cryosphere meltwater on runoff in an inland river basin of China. Global and Planetary Change 143, 189-195.
Lin, C.Y., Abdullah, M.H., Praveena, S.M., Yahaya, A.H.B., Musta, B., 2012. Delineation of temporal variability and governing factors influencing the spatial variability of shallow groundwater chemistry in a tropical sedimentary island. Journal of Hydrology 432, 26-42.
Ma, J., Ding, Z., Edmunds, W.M., Gates, J.B., Huang, T., 2009. Limits to recharge of groundwater from Tibetan

plateau to the Gobi desert, implications for water management in the mountain front. Journal of Hydrology 364, 128-141.
Mativenga, P.T., Marnewick, A., 2018. Water quality in a mining and water-stressed region. Journal of Cleaner Production 171, 446-456.
Matson, P.A., Parton, W.J., Power, A., Swift, M., 1997. Agricultural intensification and ecosystem properties. Science 277, 504-509.
Mayer, B., Boyer, E.W., Goodale, C., Jaworski, N.A., Van Breemen, N., Howarth, R.W., Seitzinger, S., Billen, G., Lajtha, K., Nadelhoffer, K., 2002. Sources of nitrate in rivers draining sixteen watersheds in the northeastern US: Isotopic constraints. Biogeochemistry 57, 171-197.
Nordin, A.P., Da Silva, J., de Souza, C.T., Niekraszewicz, L.A., Dias, J.F., da Boit, K., Oliveira, M.L., Grivicich, I., Garcia, A.L.H., Oliveira, L.F.S., 2018. In vitro genotoxic effect of secondary minerals crystallized in rocks from coal mine drainage. Journal of Hazardous Materials 346, 263-272.
Novotny, V., 2003. Water quality: diffuse pollution and watershed management. John Wiley & Sons.
Oliveira, M.L., Da Boit, K., Schneider, I.L., Teixeira, E.C., Borrero, T.J.C., Silva, L.F., 2018. Study of coal cleaning rejects by FIB and sample preparation for HR-TEM: Mineral surface chemistry and nanoparticle-aggregation control for health studies. Journal of Cleaner Production 188, 662-669.
Oliveira, M.L., Saikia, B.K., da Boit, K., Pinto, D., Tutikian, B.F., Silva, L.F., 2019. River dynamics and nanopaticles formation: A comprehensive study on the nanoparticle geochemistry of suspended sediments in the Magdalena River, Caribbean Industrial Area. Journal of Cleaner Production 213, 819-824.
Oliveira, M.L., Ward, C.R., Izquierdo, M., Sampaio, C.H., de Brum, I.A., Kautzmann, R.M., Sabedot, S., Querol, X., Silva, L.F., 2012. Chemical composition and minerals in pyrite ash of an abandoned sulphuric acid production plant. Science of the Total Environment 430, 34-47.
Pacyna, J.M., Pacyna, E.G., 2001. An assessment of global and regional emissions of trace metals to the atmosphere from anthropogenic sources worldwide. Environmental Reviews 9, 269-298.
Painter, T.H., Deems, J.S., Belnap, J., Hamlet, A.F., Landry, C.C., Udall, B., 2010. Response of Colorado River runoff to dust radiative forcing in snow. Proceedings of the National Academy of Sciences.
Plank, T., Langmuir, C.H., 1993. Tracing trace elements from sediment input to volcanic output at subduction zones. Nature 362, 739.
Ramos, C.G., Querol, X., Dalmora, A.C., de Jesus Pires, K.C., Schneider, I.A.H., Oliveira, L.F.S., Kautzmann, R.M., 2017. Evaluation of the potential of volcanic rock waste from southern Brazil as a natural soil fertilizer. Journal of Cleaner Production 142, 2700-2706.
Rascher, E., Rindler, R., Habersack, H., Sass, O., 2018. Impacts of gravel mining and renaturation measures on the sediment flux and budget in an alpine catchment (Johnsbach Valley, Austria). Geomorphology 318, 404-420.
Rivett, M.O., Buss, S.R., Morgan, P., Smith, J.W., Bemment, C.D., 2008. Nitrate attenuation in groundwater: a review of biogeochemical controlling processes. Water Research 42, 4215-4232.
Rodriguez-Iruretagoiena, A., de Vallejuelo, S.F.-O., de Diego, A., de Leão, F.B., de Medeiros, D., Oliveira, M.L., Tafarel, S.R., Arana, G., Madariaga, J.M., Silva, L.F., 2016. The mobilization of hazardous elements after a tropical storm event in a polluted estuary. Science of the Total Environment 565, 721-729.
Sánchez-Peña, N.E., Narváez-Semanate, J.L., Pabón-Patiño, D., Fernández-Mera, J.E., Oliveira, M.L., da Boit, K., Tutikian, B.F., Crissien, T.J., Pinto, D.C., Serrano, I.D., 2018. Chemical and nano-mineralogical study for determining potential uses of legal Colombian gold mine sludge: Experimental evidence. Chemosphere 191, 1048-1055.
Sanchís, J., Oliveira, L.F.S., De Leão, F.B., Farré, M., Barceló, D., 2015. Liquid chromatography–atmospheric pressure photoionization–Orbitrap analysis of fullerene aggregates on surface soils and river sediments from Santa Catarina (Brazil). Science of the Total Environment 505, 172-179.
Scanlon, B.R., Jolly, I., Sophocleous, M., Zhang, L., 2007. Global impacts of conversions from natural to agricultural ecosystems on water resources: Quantity versus quality. Water Resources Research 43.
Scheidegger, A.E., 1965. The algebra of stream-order numbers. United States Geological Survey Professional Paper 525, 187-189.
Shaffer, D.L., Tousley, M.E., Elimelech, M., 2017. Influence of polyamide membrane surface chemistry on gypsum scaling behavior. Journal of Membrane Science 525, 249-256.
Silva, L.F., de Vallejuelo, S.F.-O., Martinez-Arkarazo, I., Castro, K., Oliveira, M.L., Sampaio, C.H., de Brum, I.A., de Leão, F.B., Taffarel, S.R., Madariaga, J.M., 2013. Study of environmental pollution and mineralogical characterization of sediment rivers from Brazilian coal mining acid drainage. Science of the Total Environment 447, 169-178.
Smolders, A.J., Lucassen, E.C., Bobbink, R., Roelofs, J.G., Lamers, L.P., 2010. How nitrate leaching from

agricultural lands provokes phosphate eutrophication in groundwater fed wetlands: the sulphur bridge. Biogeochemistry 98, 1-7.
Strahler, A.N., 1957. Quantitative analysis of watershed geomorphology. Eos, Transactions American Geophysical Union 38, 913-920.
Tian, Y., Xiong, J., He, X., Pi, X., Jiang, S., Han, F., Zheng, Y., 2018. Joint operation of surface water and groundwater reservoirs to address water conflicts in arid regions: An integrated modeling study. Water 10, 1105.
Tilman, D., Cassman, K.G., Matson, P.A., Naylor, R., Polasky, S., 2002. Agricultural sustainability and intensive production practices. Nature 418, 671.
Tiwari, A.K., De Maio, M., Singh, P.K., Mahato, M.K., 2015. Evaluation of surface water quality by using GIS and a heavy metal pollution index (HPI) model in a coal mining area, India. Bulletin of Environmental Contamination and Toxicology 95, 304-310.
Tiwary, R., Kumari, B., Singh, D., 2018. Water Quality Assessment and Correlation Study of Physico-Chemical Parameters of Sukinda Chromite Mining Area, Odisha, India. Environmental Pollution. Springer, pp. 357-370.
Tüfekci, N., Sivri, N., Toroz, İ., 2007. Pollutants of textile industry wastewater and assessment of its discharge limits by water quality standards. Turkish Journal of Fisheries and Aquatic Sciences 7.
Vörösmarty, C.J., McIntyre, P.B., Gessner, M.O., Dudgeon, D., Prusevich, A., Green, P., Glidden, S., Bunn, S.E., Sullivan, C.A., Liermann, C.R., 2010. Global threats to human water security and river biodiversity. Nature 467, 555.
Wang, N., Zhang, S., He, J., Pu, J., Wu, X., Jiang, X., 2009. Tracing the major source area of the mountainous runoff generation of the Heihe River in northwest China using stable isotope technique. Chinese Science Bulletin 54, 2751-2757.
Wei, W., Ma, R., Sun, Z., Zhou, A., Bu, J., Long, X., Liu, Y., 2018. Effects of mining activities on the release of heavy metals (HMs) in a typical mountain headwater region, the Qinghai-Tibet Plateau in China. International journal of environmental research and public health 15, 1987.
Wellen, C., Shatilla, N.J., Carey, S.K., 2018. The influence of mining on hydrology and solute transport in the Elk Valley, British Columbia, Canada. Environmental Research Letters 13, 074012.
Zhao, L., Yin, L., Xiao, H., Cheng, G., Zhou, M., Yang, Y., Li, C., Zhou, J., 2011. Isotopic evidence for the moisture origin and composition of surface runoff in the headwaters of the Heihe River basin. Chinese Science Bulletin 56, 406-415.
Zhu, B., Yang, X., 2007. The ion chemistry of surface and ground waters in the Taklimakan Desert of Tarim Basin, western China. Chinese Science Bulletin 52, 2123-2129.

Declaration of interests

☒ The authors declare that they have no known competing financial interests or personal relationships that could have appeared to influence the work reported in this paper.

☐The authors declare the following financial interests/personal relationships which may be considered as potential competing interests:

Highlights

*Geographical characteristics of topography and mining activity strongly influence mining pollution in alpine catchments

*Heavy metal distributions that account topographic patterning allow for spatial interpolation

*Water chemical parameters can be reasonable predictors to trace soil mining pollution

*Relationships between water chemical parameters and soil heavy metals can help understand the mining pollution process